

## Research Article

## The binding and structural basis of fox ACE2 to RBDs from different sarbecoviruses

Junsen Chen<sup>a</sup>, Junqing Sun<sup>b,c</sup>, Zepeng Xu<sup>b,d</sup>, Linjie Li<sup>b</sup>, Xinrui Kang<sup>b</sup>, Chunliang Luo<sup>b</sup>, Qi Wang<sup>a</sup>, Xueyang Guo<sup>a</sup>, Yan Li<sup>b</sup>, Kefang Liu<sup>c,\*</sup>, Ying Wu<sup>a,\*</sup><sup>a</sup> State Key Laboratory of Virology and Hubei Province Key Laboratory of Allergy and Immunology, Institute of Medical Virology, TaiKang Medical School (School of Basic Medical Sciences), Wuhan University, Wuhan, 430071, China<sup>b</sup> CAS Key Laboratory of Pathogen Microbiology and Immunology, Institute of Microbiology, Chinese Academy of Sciences, Beijing, 100101, China<sup>c</sup> Beijing Life Science Academy, Beijing, 102209, China<sup>d</sup> Faculty of Health Sciences, University of Macau, Macau, SAR, 999078, China

## ARTICLE INFO

## Keywords:

Sarbecoviruses  
SARS-CoV  
SARS-CoV-2  
Fox ACE2  
Omicron  
Cryo-EM structure

## ABSTRACT

Foxes are susceptible to SARS-CoV-2 in laboratory settings, and there have also been reports of natural infections of both SARS-CoV and SARS-CoV-2 in foxes. In this study, we assessed the binding capacities of fox ACE2 to important sarbecoviruses, including SARS-CoV, SARS-CoV-2, and animal-origin SARS-CoV-2 related viruses. Our findings demonstrated that fox ACE2 exhibits broad binding capabilities to receptor-binding domains (RBDs) of sarbecoviruses. We further determined the cryo-EM structures of fox ACE2 complexed with RBDs of SARS-CoV, SARS-CoV-2 prototype (PT), and Omicron BF.7. Through structural analysis, we identified that the K417 mutation can weaken the ability of SARS-CoV-2 sub-variants to bind to fox ACE2, thereby reducing the susceptibility of foxes to SARS-CoV-2 sub-variants. In addition, the Y498 residue in the SARS-CoV RBD plays a crucial role in forming a vital cation- $\pi$  interaction with K353 in the fox ACE2 receptor. This interaction is the primary determinant for the higher affinity of the SARS-CoV RBD compared to that of the SARS-CoV-2 PT RBD. These results indicate that foxes serve as potential hosts for numerous sarbecoviruses, highlighting the critical importance of surveillance efforts.

## 1. Introduction

SARS-CoV-2, the causative agent of coronavirus disease 2019 (COVID-19) pandemic, has been circulating in the human population for nearly four years, and infecting hundreds of millions of people (Zhu et al., 2020; Wang et al., 2020). Since the early stages of the COVID-19 pandemic, there has been significant attention on the potential host range of SARS-CoV-2. Comparative and structural analysis of the cell receptor angiotensin-converting enzyme 2 (ACE2) in vertebrates has indicated that SARS-CoV-2 may have a broad host range (Rao et al., 2023). Studies on the receptor binding and pseudovirus of the SARS-CoV-2 prototype (PT) have shown that ACE2s from various species can bind to the SARS-CoV-2 receptor binding domain (RBD) and facilitate the infection of SARS-CoV-2 pseudovirus (Wu et al., 2020; Liu K. et al., 2021; Tang et al., 2022; Wang et al., 2023). Furthermore, SARS-CoV-2 continues to evolve into numerous sub-variants (Xu et al., 2022b). Our previous research indicated that Omicron has expanded its

receptor binding spectra (Li et al., 2022). It has now been discovered that multiple species, both naturally and experimentally, can be infected with SARS-CoV-2 and its sub-variants (Cui et al., 2022; Gao and Wang, 2021). Multiple adaptive mutations have been observed following spillover from humans to animals, leading to increased diversity in SARS-CoV-2 variants (Kane et al., 2023).

Receptor binding is a crucial step in the infection process of SARS-CoV-2 (Wang et al., 2020; Yan et al., 2020; Peng et al., 2021; Zhao et al., 2023). Consequently, the binding ability of SARS-CoV-2 to the host ACE2 receptor is a pivotal indicator for assessing the susceptibility of hosts to SARS-CoV-2 and other coronavirus (CoVs). Fox ACE2 shares approximately 85% amino acid identity with human ACE2 (hACE2). Previous research suggests that the binding affinities of SARS-CoV and SARS-CoV-2 receptor-binding domains (RBDs) to fox ACE2 are comparable to that of hACE2 (Wu et al., 2020). Additionally, fox ACE2 has demonstrated the ability to bind to RBDs from animal-origin SARS-CoV-2 related viruses, such as RaTG13, GX/P2V/2017, GD/1/2019, and

\* Corresponding authors.

E-mail addresses: [yingwu@whu.edu.cn](mailto:yingwu@whu.edu.cn) (Y. Wu), [Liukf@im.ac.cn](mailto:Liukf@im.ac.cn) (K. Liu).<https://doi.org/10.1016/j.virs.2024.06.004>

Received 19 March 2024; Accepted 6 June 2024

Available online 10 June 2024

1995-820X/© 2024 The Authors. Publishing services by Elsevier B.V. on behalf of KeAi Communications Co. Ltd. This is an open access article under the CC BY-NC-ND license (<http://creativecommons.org/licenses/by-nc-nd/4.0/>).

RshSTT182/200, indicating that foxes potentially serve as reservoirs for SARS-CoV-2 and its related CoVs (Hu et al., 2023; Niu et al., 2022; Liu Y. et al., 2021).

As early as 2005, the RNA of a SARS-CoV-like virus was detected in five red foxes (*Vulpes vulpes*) using real-time polymerase chain reaction (RT-PCR) (Wang et al., 2005). Infection experiments have shown that SARS-CoV-2-infected red foxes can shed infectious virus in both oral and nasal secretions for multiple days (Porter et al., 2022). Furthermore, SARS-CoV-2 infection in a fox was reported in September 2022 by the World Organization for Animal Health (OIE) (WOAH, 2023). Thus, elucidating the structural basis of fox ACE2 recognizing SARS-CoV-2 RBD is crucial for guiding epidemiological surveillance and spillover prevention.

In this study, we assessed the binding affinities of RBDs from seven sarbecoviruses and thirteen variants of SARS-CoV-2 to fox ACE2 and determined cryo-EM structures of SARS-CoV RBD, SARS-CoV-2 prototype (PT) RBD and Omicron BF.7 RBD in complex with fox ACE2. This study highlights the potential risk of sarbecoviruses infection in foxes.

## 2. Materials and methods

### 2.1. Cells

HEK293F suspension-cultured cells (Gibco, Cat# 11625–019, Grand Island, USA) were cultured in SMM 293-TII expression medium (Sino Biological, Cat# M293TII, Beijing, China) at 37 °C. HeLa-fox ACE2 cell line and HeLa cells were cultured as described in our previous work (Hu et al., 2023).

### 2.2. Gene cloning

The coding sequences of the SARS-CoV RBD (residues 306–527, GenBank: NC\_004718), SARS-CoV-2 PT RBD (residues 319–541, GISAID: EPI\_ISL\_402119), RaTG13-RBD (residues 319–541, GenBank: QHR63300.2), RshSTT182 RBD (residues 306–523, GISAID: EPI\_ISL\_852604), BANAL236-RBD (residues R319-F541, GISAID: EPI\_ISL\_4302647), GX/P2V/2017-RBD (residues R319-F541, GISAID: EPI\_ISL\_410542), GD/1/2019-RBD (residues R319-F541, GISAID: EPI\_ISL\_410721), mutated SARS-CoV-2 PT-RBDs (K417 N, N501Y, Y505H, A475P, Q498Y, K417T, N501T) and VOC RBDs: residues 319–541, Alpha: EPI\_ISL\_683466, Beta: EPI\_ISL\_678615, Gamma: EPI\_ISL\_833172, Delta: EPI\_ISL\_2020954, Omicron BA.1: EPI\_ISL\_6640916, Omicron BA.2: EPI\_ISL\_9845731, BA.4/5: EPI\_ISL\_12029894, Omicron BA.2.75 (BA.2 mutation D339H, G446S, N460K, R493Q), Omicron BA.2.12.1 (BA.2 mutation L452Q), BF.7 (BA.4/5 mutation R346T), BQ.1.1: EPI\_ISL\_16098101, XBB, EPI\_ISL\_16096636, XBB.1.5 (XBB mutation S486P) were fused with a C-terminal His-tag, and cloned into the pCAGGS vector. The gene encoding fox ACE2 (residues 19–615, NCBI Reference Sequence: XP\_025842512.1) was also cloned into pCAGGS vector.

### 2.3. Protein expression and purification

The fox ACE2 and RBDs were cloned into pCAGGS vectors and expressed in HEK293F cells. Following expression, the cell culture supernatants were collected and subjected to filtration through 0.22 µm filters. The purified proteins were then obtained using a purification process involving His-Trap HP chromatography (GE Healthcare) and Superdex™ 200 Increase 10/300 GL chromatography (GE Healthcare). Finally, the purified proteins were stored in a protein buffer containing 20 mM Tris-HCl (pH 8.0) and 150 mM NaCl to maintain their stability and integrity.

To form the complex of fox ACE2 with PT RBD, Omicron BF.7 RBD, and SARS-CoV RBD, the purified fox ACE2 and the three RBD proteins were mixed in a 1:2 M ratio. The mixture was then incubated for 1 h on ice to allow for proper binding. After incubation, the mixtures were subjected to purification using a Superdex™ 200 10/300 GL column (GE

Healthcare) in a buffer containing 20 mM Tris-HCl (pH 8.0) and 150 mM NaCl. The peak representing the complex was collected, and the sample was concentrated to approximately 2 mg/mL to prepare for cryo-EM analysis.

### 2.4. Surface plasmon resonance (SPR) analysis

The binding affinity of the RBDs for fox ACE2 was measured by SPR in single-cycle mode using a BIAcore 8K (GE Healthcare). All the protein buffers were transferred into PBS (Phosphate buffer, pH 7.4), and PBST (PBS, pH 7.4, 0.5% (v/v) Tween-20) was used as the running buffer. Fox ACE2 proteins were immobilized on CM5 sensors (GE Healthcare). As the flow phases, various RBDs were doubly diluted into five stages of concentration and then interacted with the CM5 sensor using a single cycle mode generated by the BIAcore 8K control system.

Binding studies were conducted using BIAcore 8K Evaluation Software (GE Healthcare) to obtain the  $K_D$  values for SPR experiments, utilizing a 1:1 binding model. The values presented are the mean ± standard deviation (SD) of three replicates.

### 2.5. Pseudovirus assay

The construction of VSV-ΔG-GFP-based RaTG13, GD/1/2019, SARS-CoV, PT, Omicron BA.1 and Omicron BF.7 pseudoviruses were described in our previous work (Zhao et al., 2021). Additionally, the establishment of the HeLa cell line expressing fox ACE2 was also described in our previous work (Hu et al., 2023).

For the infection assays, the pseudovirus particles were first normalized to the same amounts by qRT-PCR quantitation (Li et al., 2022; Hu et al., 2023). The pseudoviruses were treated with 0.5 U/mL BaseMuncher endonuclease (Abcam, Cat# ab270049, Cambridge, United Kingdom) for 1 h at 37 °C to remove nucleic acid before quantitation. Viral RNA was extracted (Bioer Technology, Cat# BYQ6.6.101711–213, Hangzhou, China) and quantified by quantitative RT-PCR (qPCR) using a 7500 fast Real-Time PCR System (Applied Biosystems) with the primers and probe for detecting the *L* gene of VSV. Then, equivalent amounts of pseudovirus were added to each well of 96-well plates containing the HeLa-fox ACE2 cell line. HeLa cells were used as a control. The numbers of fluorescent cells were calculated on a CQ1 confocal image cytometer (Yokogawa) after 15–18 h of infection. Each group contains eight parallel experiments.

### 2.6. Cryo-EM sample preparation and data acquisition

To prepare the cryo sample, the fox ACE2/PT RBD, fox ACE2/Omicron BF.7 RBD or fox ACE2/SARS-CoV RBD complex sample was vitrified using a Vitrobot Mark IV (ThermoFisher Scientific) plunge freezing device. The sample (4.0 µL, 0.1 mg/ml) was applied to graphene oxide (GO) coated grids (R1.2/1.3300 mesh). Grids above were then blotted using different conditions (blot time 2 s and blot force –2; blot time 2 s and blot force –4) at a temperature of 4 °C and a humidity level of >99% and plunge frozen into liquid ethane.

The prepared grids were transferred to a 300 kV Titan Krios transmission electron microscope equipped with Gatan K3 detector and GIF Quantum energy filter. Movies were collected at 105,000 × magnification with a calibrated pixel size of 0.69 Å over a defocus range of –1.0 µm to –2.0 µm in super resolution counting mode with a total dose of 60 e<sup>–</sup>/Å<sup>2</sup> using EPU (ThermoFisher Scientific) automated acquisition software.

### 2.7. Image processing

The detailed data processing workflow is summarized in [Supplementary Table S1](#). All the raw dose-fractionated images stacks were 2 × binned, aligned, dose-weighted and summed using MotionCor2 (Zheng et al., 2017). The contrast transfer function (CTF) estimation, particle

picking and extraction, 2D classification, ab initio model generation, 3D refinements were performed in cryoSPARC v. 4.2.0 (Punjani et al., 2017).

For the fox ACE2/PT RBD complex, a total of 7904 micrographs were collected for this dataset. We picked out particles using blob-pick procedure of cryoSPARC from 1000 micrographs, and then these particles were subjected to 2D classification. After three rounds of 2D classification, we selected good particles in different views for Topaz training and then generated the Topaz model. Then we applied the Topaz procedure to select particles against entire micrographs (Bepler et al., 2019). The 1,289,954 initial particles were picked and extracted with the box size of 256 pixels from 7904 micrographs. After the extensive 2D classification, approximately 918,772 good particles were selected to generate the initial models and two rounds of Heterogeneous Refinement and resulted to six distinct volumes. The two dominant class containing 17 % and 23 % of total particles was identified, which displayed clear features of secondary structural elements, especially in the binding interface of the fox ACE2 and SARS-CoV-2 RBD. These particles were subjected to non-uniform and CTF refinements in cryoSPARC v.3.3.1, which yielded a final density map at 2.96 Å resolution estimated by the gold-standard Fourier shell correlation (FSC) cut-off value of 0.143. The final map was sharpened by DeepEMhancer.

## 2.8. Model building and structure refinement

The fox ACE2/PT RBD structures protein were rigidly docked into the density map using Chimera (Pettersen et al., 2004), Mutation and manual adjustment were carried out with Coot v.0.9.3 (Emsley et al., 2010). Glycans were added at N-linked glycosylation sites in Coot. Each residue was manually checked with the chemical properties taken into consideration during model building. Several rounds of the real-space refinement in Phenix-1.20.1 and manually building in Coot were performed until the final reliable models were obtained (Adams et al., 2010). Mol-probity was used to validate geometry and check structure quality (Chen et al., 2010). Statistics associated with data collection, 3D reconstruction and model building were summarized in Supplementary Table S1. Figures were generated using Chimera and PyMol v.2.0 (<http://www.pymol.org>) (Pettersen et al., 2004). The processing protocols for fox ACE2/Omicron BF.7 RBD and fox ACE2/SARS-CoV RBD complexes were consistent with those described above. Details of the parameters are summarized in Supplementary Table S1 and Supplementary Figs. S4–S6. The structure was analyzed using PyMOL (<https://pymol.org/2/>).

## 3. Results

### 3.1. The binding affinities of fox ACE2 to RBDs from different sarbecoviruses

Structure-based sequence alignments demonstrated that RBDs from three bat-derived CoVs (RaTG13, RshSTT182 and BANAL236) (Hu et al., 2023; Liu Y. et al., 2021), two pangolin-derived CoVs (GD/1/2019 and GX/P2V/201) (Niu et al., 2022), SARS-CoV and SARS-CoV-2 PT exhibit a high degree of conservation, but also display variations at known key sites such as site 417, 493, 498, and 501 (Supplementary Fig. S1A). Additionally, SARS-CoV-2 continues to evolve into numerous sub-variants (Supplementary Fig. S1B).

We identified two fox ACE2 orthologs, the red fox (*Vulpes vulpes*) and the arctic fox (*Vulpes lagopus*), from the National Center for Biotechnology Information (NCBI). Through sequence alignment, we observed only six differing amino acid residues between them, none of which are located on the binding interface between ACE2 and RBDs (Supplementary Fig. S2). Therefore, we chose the red fox as the representative for our study.

To evaluate the binding affinities of these RBDs to fox ACE2, we conducted SPR assays. Overall, fox ACE2 was able to bind to RBDs of all the tested sarbecoviruses with varied affinities. Notably, the binding affinities of the RBDs from BANAL236, GD/1/2019 and SARS-CoV were

even higher than that of SARS-CoV-2 PT RBD. On the other hand, the binding affinities of the RBDs from RaTG13, RshSTT182 and GX/P2V/2017 were remarkably weaker ( $K_D > 100$  nM) than those from the aforementioned sarbecoviruses (Fig. 1, Supplementary Fig. S3). For the SARS-CoV-2 sub-variants' RBDs, the affinities of Alpha RBD ( $K_D = 25.7 \pm 0.8$  nM) and Delta RBD ( $K_D = 37.7 \pm 0.9$  nM) to fox ACE2 were slightly higher than PT RBD ( $K_D = 47.1 \pm 2.0$  nM), while Beta RBD ( $K_D = 179 \pm 2.8$  nM) and Gamma RBD ( $K_D = 408 \pm 1.2$  nM) showed significantly weaker affinities to fox ACE2 than PT RBD. The RBDs from Omicron sub-variants, in particular, showed notably weaker affinities ( $K_D > 100$  nM) than the PT RBD (Fig. 1B and C).

### 3.2. Cell infectivity of pseudoviruses mediated by fox ACE2

We then examined the infectivity of VSV-based RaTG13, GD/1/2019, SARS-CoV, PT, Omicron BA.1 or Omicron BF.7 pseudoviruses to fox ACE2-expressing cells, respectively. HeLa cells overexpressing fox ACE2 (HeLa-fox-ACE2 cells) were exposed to each pseudovirus in equivalent doses (quantified by qPCR) (Fig. 2A and C), while HeLa cells lacking fox ACE2 expression served as negative controls (Fig. 2B and D). Our results indicated that all six pseudoviruses successfully entered HeLa-fox ACE2 cells. Interestingly, pseudoviruses RaTG13 exhibited significantly lower infection efficiency, whereas the pseudoviruses GD/1/2019 and SARS-CoV demonstrated notably higher efficiency compared to PT. Additionally, Omicron BA.1 and Omicron BF.7 pseudoviruses displayed relatively lower infection efficiency compared to PT pseudovirus (Fig. 2C).

### 3.3. Overall architectures of fox ACE2 bound to SARS-CoV RBD, PT RBD and Omicron BF.7 RBD

To elucidate the molecular mechanisms underlying the varied affinities of fox ACE2s binding to distinct sarbecoviruses RBDs, the cryo-EM structures of the fox ACE2/PT RBD, fox ACE2/Omicron BF.7 RBD and fox ACE2/SARS-CoV RBD complexes were determined at resolutions of 2.96 Å, 3.47 Å and 3.08 Å, respectively (Fig. 3, Supplementary Table S1; S4–S6).

Key residues involved in the hydrogen bond (H-bond) and van der Waals (vdw) interaction between fox ACE2 and the RBDs were analyzed (Supplemental Table S2). The RBDs of the PT, Omicron BF.7 and SARS-CoV exhibited similar binding interface, yielding a total of 182, 156 and 165 contacts, encompassing 10, 5 and 9 H-bonds, respectively (Fig. 3, Supplemental Table S2).

The binding surface is divided into two patches (Fig. 3). There are two pairs of H-bonds between fox ACE2 and PT RBD in Patch 1 (Y34-Q493, E35-Q493) and a salt bridge (E30-K417). Seven pairs of H-bonds are observed in Patch 2 (E37-Y505, E38-Y449, Y41-T500/N501, K353-G496/G502, D355-T500) (Fig. 3A). Conversely, only five pairs of H-bonds exist between fox ACE2 and Omicron BF.7 RBD, involving three pairs in Patch 1 (T27-Y489/N487 and Y83-N487), and two pairs in Patch 2 (Y41-T500 and K353-G502). Notably, a pair of  $\pi$ - $\pi$  interactions occur between fox ACE2 and Omicron BF.7 RBD in Patch 2 (Y41 with Y501) (Fig. 3B). SARS-CoV RBD establishes nine pairs of H-bonds with fox ACE2, including three pairs in Patch 1 (one H-bond between Q19-P475 and two H-bonds between Y83-N487), and six pairs in Patch 2 (Y41-T500, Q42-Y449/Y498, K353-Y495/G496/G502). Furthermore, a cation- $\pi$  interaction is observed between fox ACE2 and SARS-CoV RBD (K353 with Y498) (Fig. 3C).

### 3.4. Structural comparison of different fox ACE2/RBD complexes

We performed an alignment comprising key sequences of PT RBD, Omicron BF.7 RBD and SARS-CoV RBD (residue numbering according to PT). Strong polar contact sites between three RBDs and fox ACE2 are highlighted below the sequences with yellow, cyan and magenta triangles, respectively (Fig. 4A). We found that T500 and G502 were

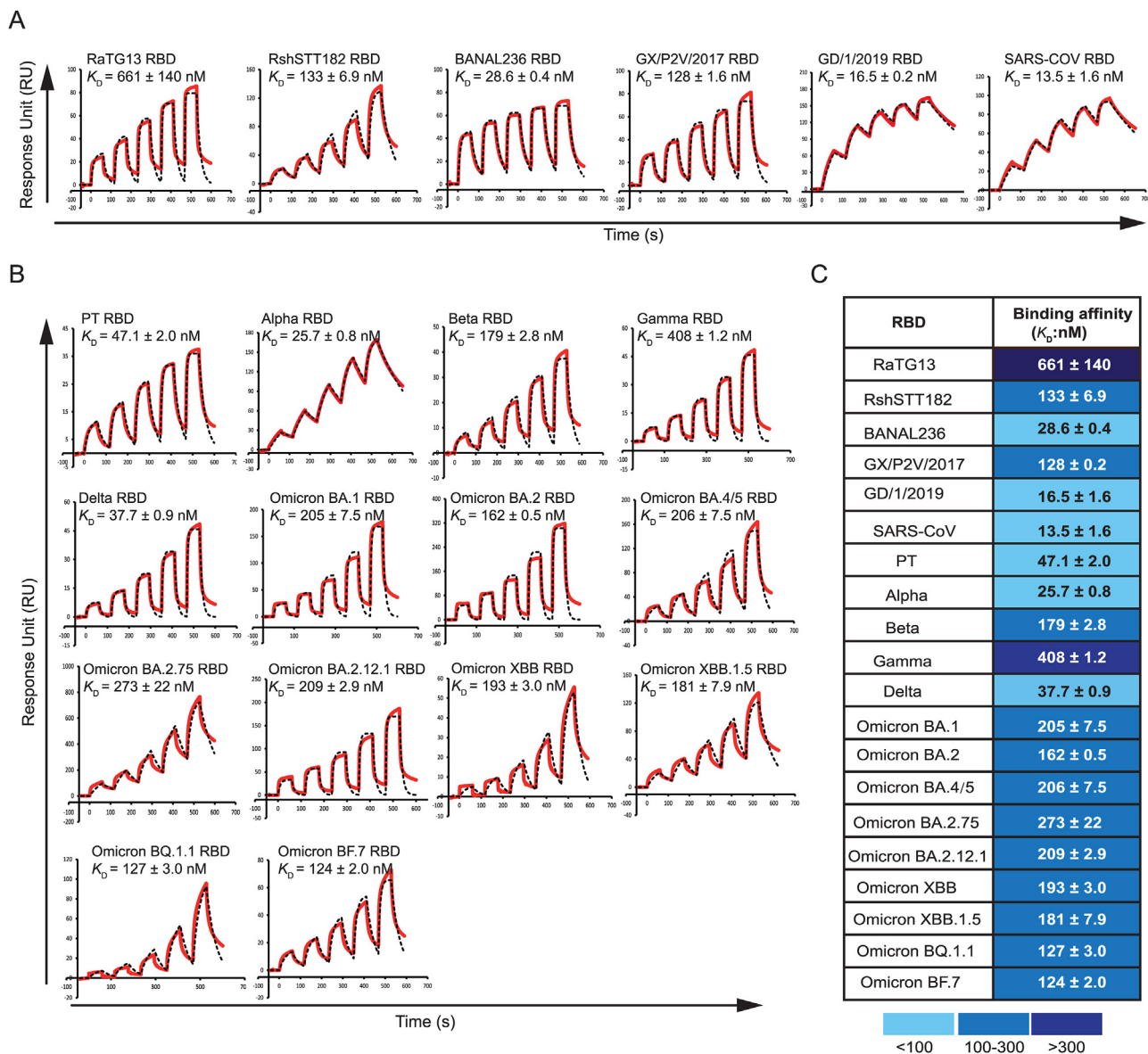


**Fig. 1.** SPR analysis of the binding affinities between fox ACE2 and RBDs from different sarbecoviruses. **A** SPR characterization of the RBDs from three bat-derived CoVs (RaTG13, RshSTT182, BANAL236), two pangolin-derived CoVs (GD/1/2019, GX/P2V/2017) and SARS-CoV interacting with fox ACE2. **B** SPR characterization of RBDs from the PT and its VOCs interacting with fox ACE2. Actual and fitted curves are colored in black and red, respectively. The  $K_D$  of each binding test is calculated from three independent repeats and are presented as mean  $\pm$  SD. Source data are provided as a Source Data file. **C** The binding affinities in (A) or (B) were presented as a heatmap according to the indicated color.

conserved across the three RBDs, participating in the formation of H-bonds in all three complex structures. Moreover, the fox ACE2/PT RBD complex revealed four unique H-bonds (K417, Q493, N501, and Y505) absent in the other two complexes. And fox ACE2/SARS-CoV RBD complex has three unique H-bonds (P475, G496 and Y498), two of which (P475 and Y498) differs from the corresponding residues in PT. In contrast, the fox ACE2/Omicron BF.7 RBD complex exhibited only one unique H-bond (Y489), and this residue is conserved among the three RBDs (Fig. 4A).

Omicron BF.7 shares 92.3% amino acid identity to PT in the RBD domain. The complex structures of the fox ACE2/Omicron BF.7 RBD and fox ACE2/PT RBD show a similar binding mode, displaying a root mean squared deviation (RMSD) of 0.434 Å for 689 C $\alpha$  atoms. We then compared the interface residues of fox ACE2/PT RBD and fox ACE2/Omicron BF.7 RBD complexes. Notably, the interface of PT RBD to fox ACE2 interaction involves five unique binding sites at K417, G466, F486, Y495 and G496, while the interaction of Omicron BF.7 RBD to fox ACE2

comprises only two unique binding sites, namely R403 and G476 (Fig. 4B, C and 4E). In addition, regarding the Omicron BF.7 RBD interface, four substitutions are found, namely S477 N, Q498R, N501Y and Y505H (Fig. 4C and E). On fox ACE2, K31 interacts with Omicron BF.7 RBD, but not with PT RBD (Fig. 4B and C).

The amino acid identity between SARS-CoV RBD and PT RBD is only 75.6%. However, the fox ACE2/SARS-CoV RBD and fox ACE2/PT RBD complexes exhibit a similar architecture, with an RMSD of 0.499 for 685 C $\alpha$  atoms. We then compared the interface residues of fox ACE2/PT RBD and fox ACE2/SARS-CoV RBD complexes. Notably, four unique binding sites of PT RBD to fox ACE2 were identified, including K417, G446, F486 and S477, while only one unique binding site (D476) of SARS-CoV RBD to fox ACE2 was observed (Fig. 4B, D and 4F). In addition, for the SARS-CoV RBD interface, six substitutions were found, namely L455Y, F456L, A475P, Q493 N, Q498Y and N501T (Fig. 4D and F). On fox ACE2, K31 and L45 interact with SARS-CoV RBD, but not with PT RBD (Fig. 4B and D).

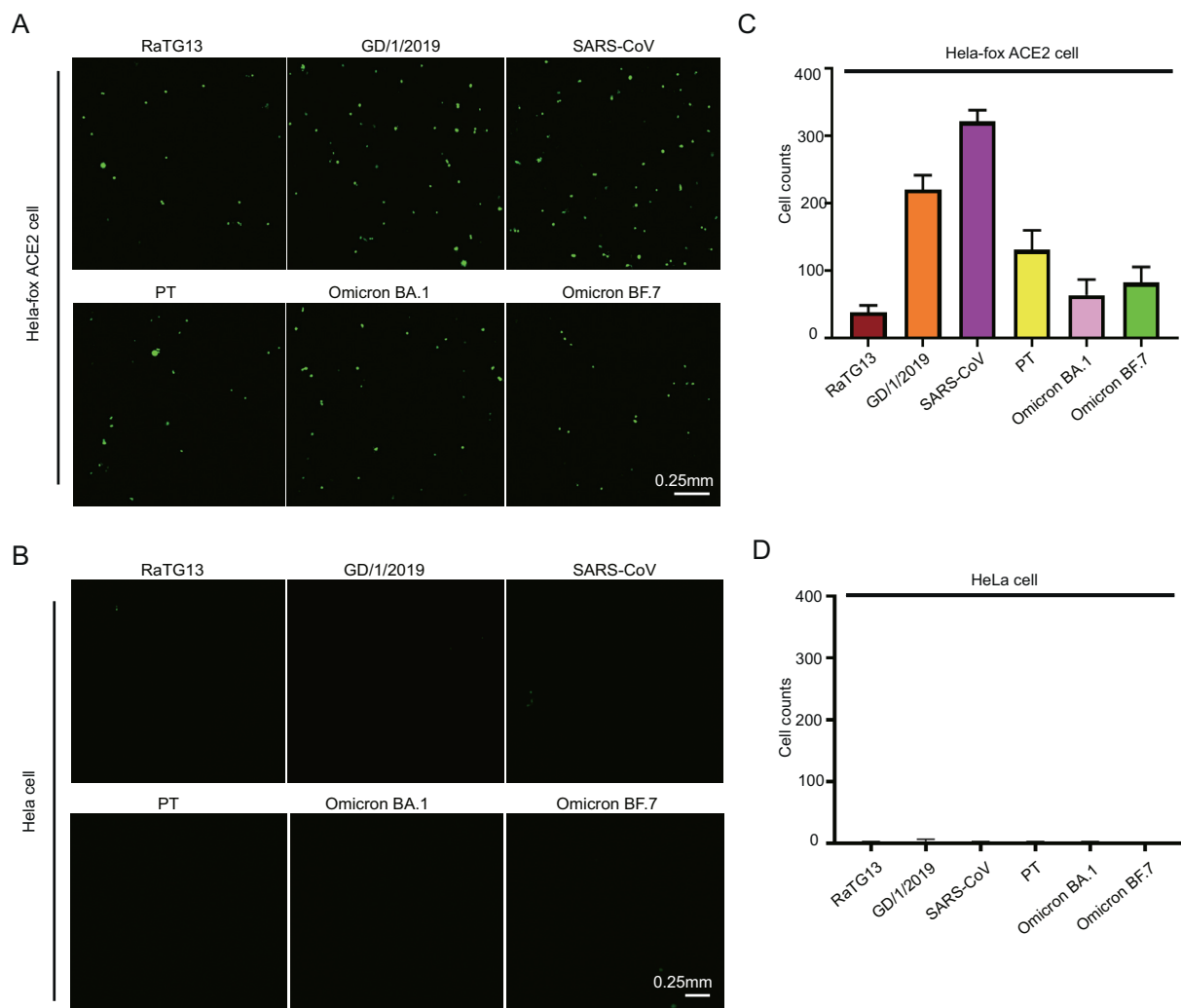


**Fig. 2.** The infectivity of RaTG13, GD/1/2019, SARS-CoV, PT, Omicron BA.1 and Omicron BF.7 pseudoviruses in HeLa cells. **A, B** HeLa-fox ACE2 cells and untransfected HeLa cells are infected with RaTG13, GD/1/2019, SARS-CoV, PT, Omicron BA.1 and Omicron BF.7 pseudoviruses, respectively. Green fluorescence indicates HeLa-fox ACE2 cells infected with pseudoviruses. The scale bar indicates 0.25 mm. **C, D** Statistic for the infectivity of the six pseudoviruses. Data represent the results of eight replicates.

### 3.5. The key residues determining the binding affinities of PT, Omicron BF.7 and SARS-CoV RBDs to fox ACE2

To investigate the molecular mechanism underlying the reduced affinity of Omicron BF.7 RBD compared to the PT RBD, we constructed three PT RBD mutants (K417 N, N501Y, and Y505H) by substituting the respective residues of PT RBD with those of Omicron BF.7 RBD, and assessed their binding affinities with fox ACE2. Of note, the PT RBD K417 N substitution exhibited approximately 10-fold weaker affinity to fox ACE2 than that of PT RBD, and the PT RBD Y505H showed approximately 2.2-fold decreased binding than that of PT RBD (Fig. 5A). On the other hand, the affinity of N501Y-RBD with fox ACE2 increased approximately 1.8-fold (Fig. 5A). Structural analysis revealed that the salt bridge between fox ACE2 E30 and PT RBD K417 is disrupted when PT RBD K417 is substituted by N417. Additionally, PT RBD Y505 forms an H-bond with E37 of fox ACE2, but when it is substituted by H505, the H-bond is broken. Consistent with the binding of N501Y-RBD to hACE2 (Xu et al., 2022a; Zhang et al., 2021), Y501 forms a  $\pi$ - $\pi$  interaction with Y41, thus enhancing the binding affinity (Fig. 5B).

On the binding interface between the Omicron BF.7 RBD and fox ACE2, two amino acids differ from the PT RBD: N477 and R498. In PT RBD, N477 forms more vdw contacts with fox ACE2 Q19 compared to

S477, whose side chain is shorter (Supplementary Fig. S7A; Table S2). Specifically, PT RBD Q498 interacts with fox ACE2 E38, Y41, and Q42 through vdw forces, while BF.7 RBD R498 engages with Y41, Q42, and L45 of fox ACE2 vdw interactions (Supplementary Fig. S7A; Table S2).

The impact of three residue substitutions (K417V, Q498Y and N501T) between SARS-CoV RBD and PT RBD on the binding affinity was also analyzed. When K417 of PT RBD was substituted with V417, the affinity to fox ACE2 decreased by more than 10-fold, while the N501T mutant exhibited 3.6-fold decrease in binding affinity (Fig. 5C). Conversely, when PT RBD Q498 was mutated to Y498, there was approximately a 4-fold increase in binding affinity (Fig. 5C). Structural alignment revealed that, similar to N417, V417 substitution can disrupt the salt bridge formed between K417 and E30 (Fig. 5D). In addition, the substitution of N501 with T501 in PT RBD hindered the formation of a hydrogen bond with Y41 of fox ACE2 (Fig. 5D). While Q498 only forms vdw interactions with E38, Y41 and Q42 of fox ACE2 (Supplementary Table S2), Y498 in SARS-CoV RBD not only forms an H-bond with Q42, but also engages in a cation- $\pi$  interaction with K353 (Fig. 5D).

Besides, there are another four amino acids on the binding interface of SARS-CoV RBD that differ from SARS-CoV-2 PT RBD, including L455Y (from SARS-CoV-2 PT RBD to SARS-CoV RBD), F456L, A475P and Q493 N. Among them, Y455, L456 and N493 form vdw interactions with fox

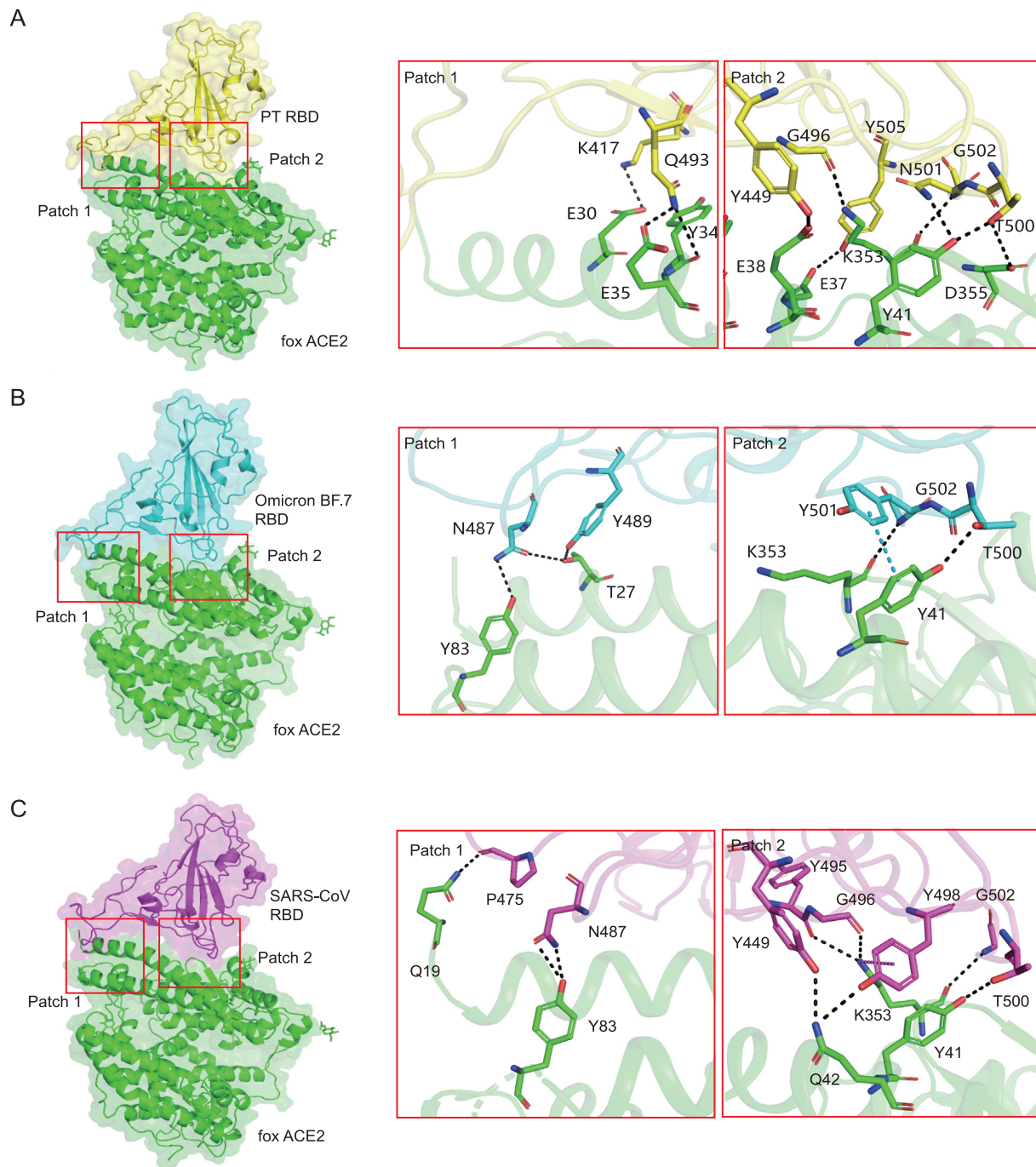


**Fig. 3.** The complex structures of PT RBD, Omicron BF.7 RBD and SARS-CoV RBD bound to fox ACE2. **A–C** The overall complex structures of fox ACE2 bound to the PT RBD (A), Omicron BF.7 RBD (B) or SARS-CoV RBD (C). The binding between the RBDs and fox ACE2 is mainly composed of two patches of interactions which are indicated in red boxes, respectively. Detailed interaction of fox ACE2 with the PT RBD (A), Omicron BF.7 RBD (B) and SARS-CoV RBD (C) are displayed in the patches, respectively. Residues involved in the interaction are labeled, and H-bond and salt bridge are shown as black dotted lines with a cutoff of 3.5 Å. There are two special interactions marked by unique dashed lines, the  $\pi$ - $\pi$  interaction in cyan (B) and the cation- $\pi$  interaction in magenta (C).

ACE2, while the N493 of PT RBD forms two pairs of H-bonds with Y34 and E35 of fox ACE2. P475 of SARS-CoV RBD forms an H-bond with Q19 of fox ACE2, which is absent in PT RBD (Supplementary Fig. S7B).

Furthermore, four additional amino acids are present on the binding interface of SARS-CoV RBD that differ from those in SARS-CoV-2 PT RBD. These variances include L455Y (from SARS-CoV-2 PT RBD to SARS-CoV RBD), F456L, A475P, and Q493N. Notably, Y455, L456, and N493 establish vdw interactions with fox ACE2, whereas N493 in PT RBD forms two sets of H-bonds with Y34 and E35 of fox ACE2. In SARS-CoV

RBD, P475 forms an H-bond with Q19 of fox ACE2, a feature absent in PT RBD (Supplementary Fig. S7B).

#### 4. Discussion

As previously reported, foxes have been found to be susceptible to both SARS-CoV and SARS-CoV-2 in nature (Wang et al., 2005; WOA, 2023). In our study, we investigated the binding of fox ACE2 to RBDs from different sarbecoviruses. Our findings revealed that fox ACE2

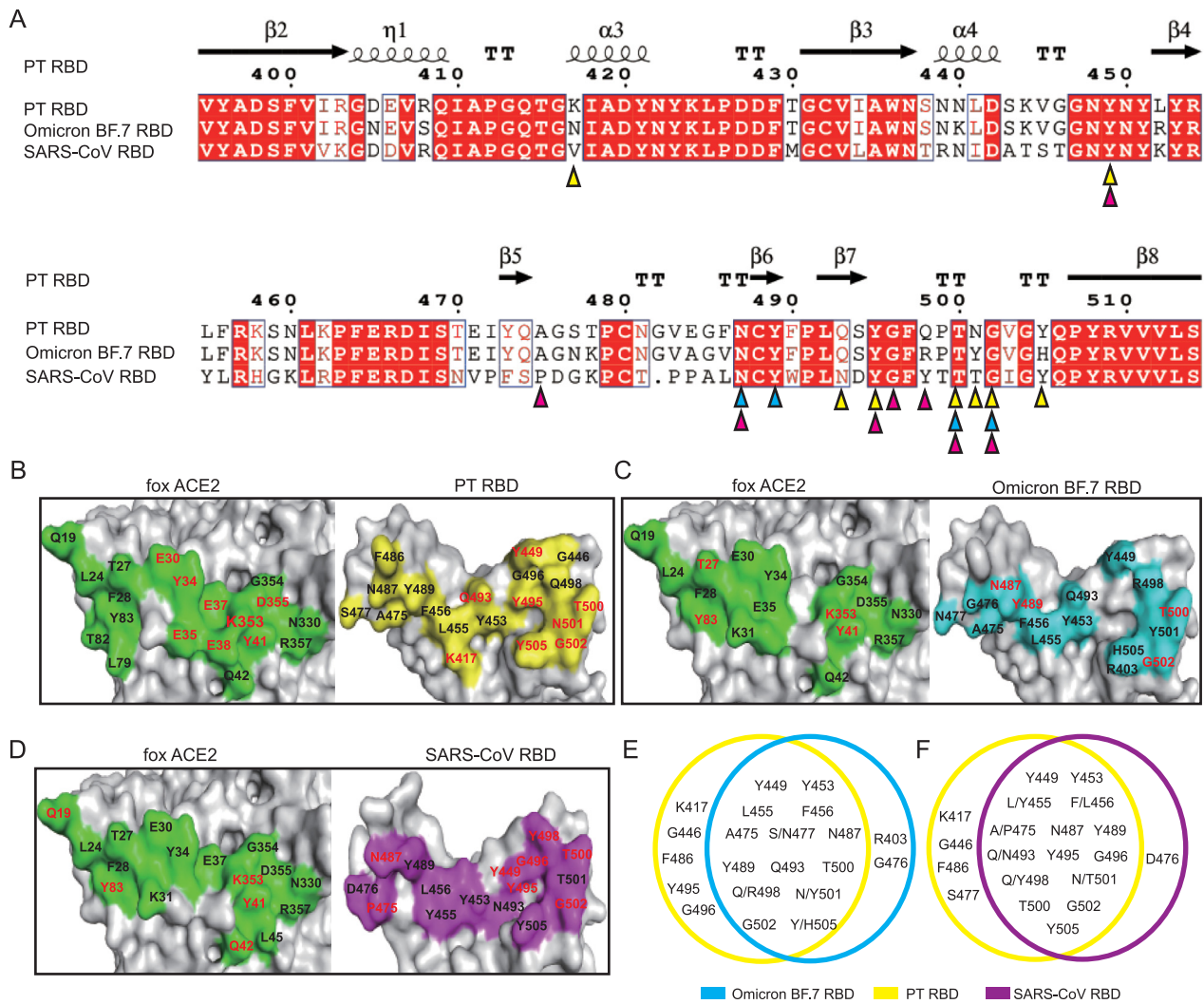


**Fig. 4.** Structural comparison of PT RBD/fox ACE2 with Omicron BF.7 RBD/fox ACE2 and SARS-CoV RBD/fox ACE2. **A** Structure-based sequence alignment of PT RBD, Omicron BF.7 RBD or SARS-CoV RBD contact with fox ACE2 through H-bonds are marked with yellow, cyan and magenta triangles, respectively. Sequence alignment is generated with Clustal X and ESPrift 3.0.cc. **B–D** Binding interface of fox ACE2/PT RBD (**B**), fox ACE2/Omicron BF.7 RBD (**C**), fox ACE2/SARS-CoV RBD (**D**). Residues involved in the interaction are labeled, and residues form H-bond, salt bridge,  $\pi$ - $\pi$ , and cation- $\pi$  are highlight in red. **E–F** Venn diagrams of key residues on PT RBD/Omicron BF.7 RBD (**E**) and PT RBD/SARS-CoV RBD (**F**) that are involved in the interaction with the fox ACE2s.

exhibited broad binding capabilities to RBDs of various sarbecoviruses. Notably, the binding affinity of fox ACE2 to the RBDs of BANAL236 and GX/P2V/2017 was even higher than that of the SARS-CoV-2 PT. Furthermore, among the 39 ACE2 orthologs we evaluated, fox ACE2 demonstrated the highest binding affinity to the RBD of RshSTT182/200 (Hu et al., 2023). These findings strongly suggest that fox could serve as important potential host for sarbecoviruses.

Residues 493, 498, and 501 within the RBD have been identified as mutational hotspots and determinants of host range (Gao and Wang, 2021). The N501Y mutation enables SARS-CoV-2 to infect mice and also enhances its binding affinity to various ACE2 orthologs, including hACE2, dog ACE2, and fox ACE2 (Zhang et al., 2021; Gu et al., 2020). Additionally, the N501T mutation strengthens the binding of the PT RBD to mink ACE2 and hACE2 (Han et al., 2021). However, in our study, we found that the N501T mutation decreases the binding affinity of the PT RBD to fox ACE2. Moreover, the Q498Y and Q498H mutations broaden the binding capabilities of the RaTG13 and GD/1/2019 strains, respectively (Niu et al., 2022; Liu K. et al., 2021). Specifically, for fox ACE2, the PT RBD Q498Y substitution increases its binding affinity.

In our previous research, we discovered that the affinities of the RBDs from SARS-CoV-2 variants to hACE2 were limited to a range of one to two digit numbers (with a dissociation constant ( $K_D$ ) of approximately 5–40 nM, normalized to the results of our laboratory for comparability) (Li et al., 2024). In this study, we observed that the binding affinities of the SARS-CoV-2 sub-variants to fox ACE2 significantly decreased, with the exception of the Alpha and Delta strains. Interestingly, all of the sub-variants that showed reduced binding to fox ACE2 possessed a K417N or K417T substitution, whereas the Alpha and Delta strains did not (Fig. 1B, Supplemental S1B and S8). The K417N substitution was found to decrease the binding affinity of RBD to dog ACE2, but had little effect on the binding of SARS-CoV-2 to hACE2 (Li et al., 2022; Zhang et al., 2021). In the GD/1/2019 RBD, R417 is present. Interestingly, the substitution in PT RBD to K417R does not significantly decrease the affinity with fox ACE2 (Supplemental Figs. S1A and S8). We speculate that this may be due to the similarity in the properties of the side chain between R417 and K417. Both residues have the ability to form a salt bridge with E30 of fox ACE2. Our findings suggest that the residue at position K417 plays a critical role in the binding of SARS-CoV-2 to fox ACE2.

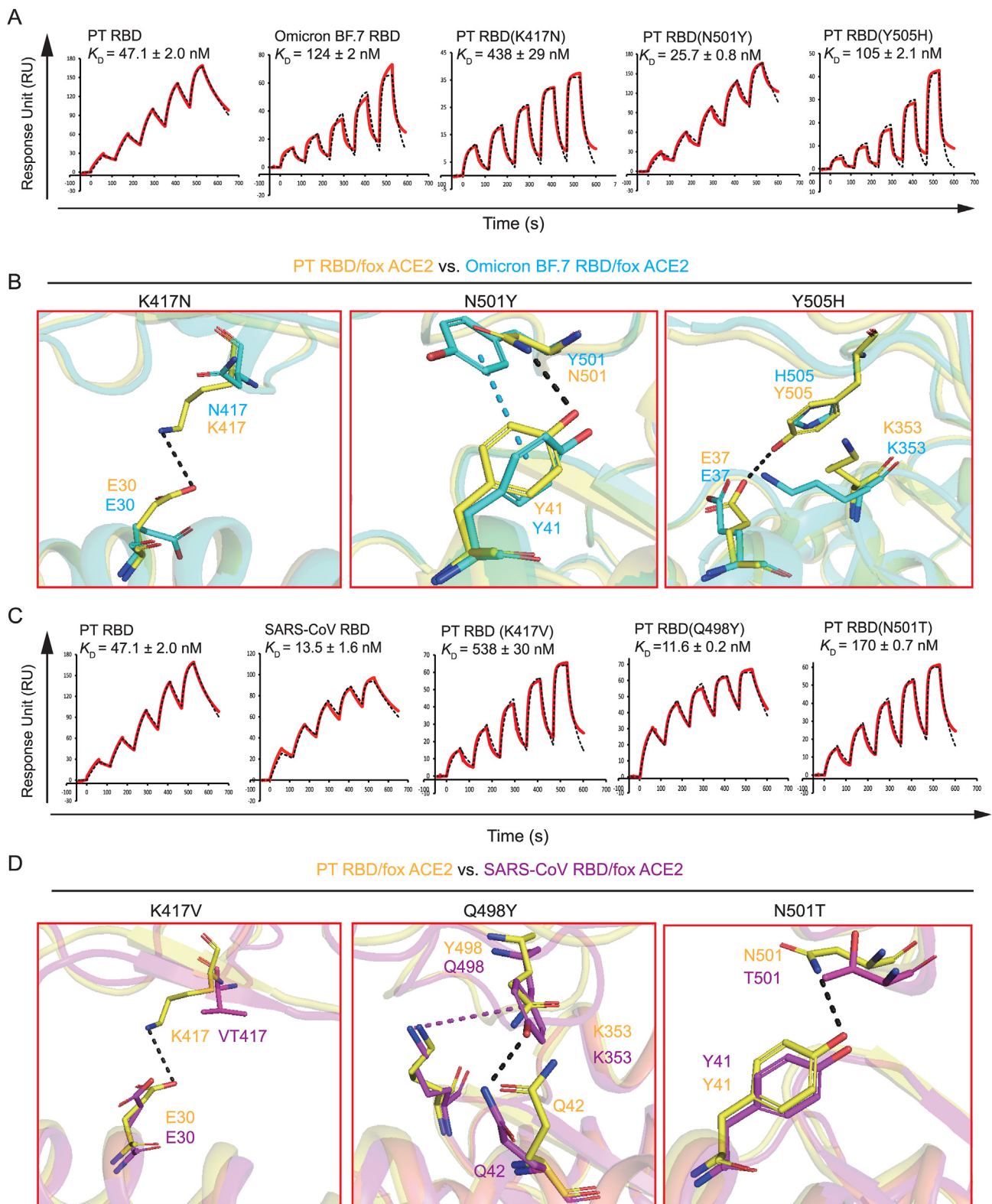


**Fig. 5.** Structural and functional analysis of key residues in the molecular interaction of fox ACE2/PT RBD, fox ACE2/Omicron BF.7 RBD and fox ACE2/SARS-CoV RBD. **A** SPR analysis of the binding affinity of RBD from Omicron BF.7 and three mutated PT strains interacting with fox ACE2. **B** Structural comparison between complexes of PT RBD and Omicron BF.7 RBD binding to the fox ACE2. **C** SPR analysis of the binding affinity of PT RBD, SARS-CoV RBD and three mutated SARS-CoV-2 RBD. **D** Structural comparison between complexes of PT RBD and SARS-CoV RBD binding to the fox ACE2. The  $K_D$  of each binding test is calculated from three independent repeats and are presented as mean  $\pm$  SD. Source data are provided as a Source Data file. Residue substitutions of the fox ACE2/PT RBD, fox ACE2/Omicron BF.7 RBD and fox ACE2/SARS-CoV RBD are colored in yellow, cyan and magenta, respectively. Residues involved in the interaction are represented as sticks and H-bonds are shown as black dotted lines with a cutoff of 3.5.  $\pi$ - $\pi$  interaction is shown as cyan dashed lines and cation- $\pi$  interaction shown as magenta dashed lines.

So far, more than 40 species have been reported to be naturally infected with SARS-CoV-2 (<https://www.fao.org/animal-health/situations-updates/sars-cov-2-in-animals/en>). In some animals, SARS-CoV-2 can spread within their species and can also spillover back to humans, such as mink and white-tailed deer (Hammer et al., 2021; Pickering et al., 2022; Han et al., 2023). However, there has been only one reported case of SARS-CoV-2 infection in foxes (WOAH, 2023). This could be due to the fact that foxes are not extensively tested for COVID-19. Another factor worth considering is that the K417 mutation may weaken the ability of the virus to bind to fox ACE2, rendering foxes less susceptible to SARS-CoV-2 sub-variants. If this is the case, foxes may no longer serve as suitable hosts for the evolution of SARS-CoV-2. It also suggests that while mutations in SARS-CoV-2 can broaden the range of host species, it may also result in a loss of infectivity towards certain species (Li et al., 2022).

There are several limitations to this study. Firstly, our focus was solely on the impact of receptor binding on viral infection. Additional research is required to examine the influence of mutations in the non-receptor binding region of the S protein on its conformation or expression level, and consequently on viral infection in the host. Furthermore, it is crucial to acknowledge that there are various other factors that can potentially affect virus infectivity, such as replication, assembly, etc.

## 5. Conclusions

Our study indicates that the fox ACE2 can bind to the RBDs of various sarbecoviruses. Additionally, we identified that the Y498 in SARS-CoV RBD can form a cation- $\pi$  interaction with K353 in fox ACE2, which is the main factor responsible for the higher affinity of SARS-CoV RBD than that of PT RBD. Moreover, the K417N and K417T mutations decrease the ability of SARS-CoV-2 sub-variants to fox ACE2. These results suggest that while mutations in SARS-CoV-2 can broaden its host range, it may also result in a loss of infectivity towards certain species. In conclusion, our study highlights the potential risk of coronavirus infection in foxes and provides an early warning of potential spillover and provides the structural basis of interspecies transmission of coronaviruses to foxes.

## Data availability

The atomic coordinates for the fox ACE2/PT RBD complex, the fox ACE2/Omicron BF.7 RBD and the fox ACE2/SARS-CoV RBD complex are deposited in the Protein Data Bank (<https://www.rcsb.org/>) with accession number of 8XYZ, 8XZD and 8XZB, respectively. The corresponding electron microscopy maps of the fox ACE2/PT RBD complex, the fox ACE2/Omicron BF.7 RBD and the fox ACE2/SARS-CoV RBD complex are deposited in the Electron Microscopy Data Bank with accession numbers EMD-38792, EMD-38793 and EMD-38784, respectively. We also deposit those data in the Science Data Bank (<https://www.scidb.cn/en>) (CSTR: 31253.11.sciencedb.09206).

## Ethics statement

This article does not contain any studies with human or animal subjects performed by any of the authors.

## Author contributions

Junsen Chen: conceptualization, data curation, formal analysis, investigation, methodology, validation, writing-original draft. Junqing Sun: data curation, methodology, validation. Zepeng Xu: methodology, resources. Linjie Li: methodology, resources. Xinrui Kang: methodology, resources. Chunliang Luo: methodology, resources. Qi Wang: methodology, resources. Xueyang Guo: methodology, resources. Yan Li: methodology, funding acquisition. Kefang Liu: conceptualization, formal analysis, funding acquisition, investigation, methodology, resources, supervision, validation, writing-review & editing. Ying Wu:

conceptualization, formal analysis, funding acquisition, investigation, methodology, resources, supervision, validation, writing-review & editing.

## Conflict of interest

The authors declare that they have no conflict of interest.

## Acknowledgements

We are grateful to X. Li, Y. Mi, W. Li, Q. Dong and E. Pang (the Cryo-EM Center, Shanxi Academy of Advanced Research and Innovation) for their technical support on cryo-EM. We thank Y. Chen, Z. Yang, B. Zhou (Institute of Biophysics, Chinese Academy of Sciences), and Z. Fan (Institute of Microbiology, Chinese Academy of Sciences) for technical help with SPR experiments. This work was supported by the National Key R&D Program of China (2022YFC2303401, 2021YFA1300803), National Natural Science Foundation of China (32122008). Kefang Liu was supported by Young Elite Scientists Sponsorship Program by CAST (2021QNRC001), fellowships from the China Postdoctoral Science Foundation (2022T150688) and the Postdoctoral Science Foundation of China (2021M700161).

## Appendix A. Supplementary data

Supplementary data to this article can be found online at <https://doi.org/10.1016/j.virs.2024.06.004>.

## References

- Adams, P.D., Afonine, P.V., Bunkóczi, G., Chen, V.B., Davis, I.W., Echols, N., Headd, J.J., Hung, L.W., Kapral, G.J., Grosse-Kunstleve, R.W., McCoy, A.J., Moriarty, N.W., Oeffner, R., Read, R.J., Richardson, D.C., Richardson, J.S., Terwilliger, T.C., Zwart, P.H., 2010. PHENIX: a comprehensive Python-based system for macromolecular structure solution. *Acta Crystallogr D Biol Crystallogr* 66, 213–221.
- Bepko, T., Morin, A., Rapp, M., Brasch, J., Shapiro, L., Noble, A.J., Berger, B., 2019. Positive-unlabeled convolutional neural networks for particle picking in cryo-electron micrographs. *Nat. Methods* 16, 1153–1160.
- Chen, V.B., Arendall, W. B., 3rd, Headd, J.J., Keedy, D.A., Immormino, R.M., Kapral, G.J., Murray, L.W., Richardson, J.S., Richardson, D.C., 2010. MolProbity: all-atom structure validation for macromolecular crystallography. *Acta Crystallogr D Biol Crystallogr* 66, 12–21.
- Cui, S., Liu, Y., Zhao, J., Peng, X., Lu, G., Shi, W., Pan, Y., Zhang, D., Yang, P., Wang, Q., 2022. An updated review on SARS-CoV-2 infection in animals. *Viruses* 14, 1527.
- Emsley, P., Lohkamp, B., Scott, W.G., Cowtan, K., 2010. Features and development of Coot. *Acta Crystallogr D Biol Crystallogr* 66, 486–501.
- Gao, G.F., Wang, L., 2021. COVID-19 expands its territories from humans to animals. *China CDC Weekly* 3, 855–858.
- Gu, H., Chen, Q., Yang, G., He, L., Fan, H., Deng, Y.Q., Wang, Y., Teng, Y., Zhao, Z., Cui, Y., Li, Y., Li, X.F., Li, J., Zhang, N.N., Yang, X., Chen, S., Guo, Y., Zhao, G., Wang, X., Luo, D.Y., Wang, H., Yang, X., Li, Y., Han, G., He, Y., Zhou, X., Geng, S., Sheng, X., Jiang, S., Sun, S., Qin, C.F., Zhou, Y., 2020. Adaptation of SARS-CoV-2 in BALB/c mice for testing vaccine efficacy. *Science* 369, 1603–1607.
- Hammer, A.S., Quaade, M.L., Rasmussen, T.B., Fonager, J., Rasmussen, M., Mundbjerg, K., Lohse, L., Strandbygaard, B., Jørgensen, C.S., Alfaro-Núñez, A., Rosenstjerne, M.W., Boklund, A., Halasa, T., Fomsgaard, A., Belsham, G.J., Bøtner, A., 2021. SARS-CoV-2 Transmission between mink (*Neovison vison*) and humans, Denmark. *Emerg. Infect. Dis.* 27, 547–551.
- Han, P., Su, C., Zhang, Y., Bai, C., Zheng, A., Qiao, C., Wang, Q., Niu, S., Chen, Q., Zhang, Y., Li, W., Liao, H., Li, J., Zhang, Z., Cho, H., Yang, M., Rong, X., Hu, Y., Huang, N., Yan, J., Wang, Q., Zhao, X., Gao, G.F., Qi, J., 2021. Molecular insights into receptor binding of recent emerging SARS-CoV-2 variants. *Nat. Commun.* 12, 6103.
- Han, P., Meng, Y., Zhang, D., Xu, Z., Li, Z., Pan, X., Zhao, Z., Li, L., Tang, L., Qi, J., Liu, K., Gao, G.F., 2023. Structural basis of white-tailed deer, *Odocoileus virginianus*, ACE2 recognizing all the SARS-CoV-2 variants of concern with high affinity. *J. Virol.* 97, e0050523.
- Hu, Y., Liu, K., Han, P., Xu, Z., Zheng, A., Pan, X., Jia, Y., Su, C., Tang, L., Wu, L., Bai, B., Zhao, X., Tian, D., Chen, Z., Qi, J., Wang, Q., Gao, G.F., 2023. Host range and structural analysis of bat-origin RshST182/200 coronavirus binding to human ACE2 and its animal orthologs. *EMBO J.* 42, e111737.
- Kane, Y., Wong, G., Gao, G.F., 2023. Animal models, zoonotic reservoirs, and cross-species transmission of emerging human-infecting coronaviruses. *Annu Rev Anim Biosci* 11, 1–31.
- Li, L., Han, P., Huang, B., Xie, Y., Li, W., Zhang, D., Han, P., Xu, Z., Bai, B., Zhou, J., Kang, X., Li, X., Zheng, A., Zhang, R., Qiao, S., Zhao, X., Qi, J., Wang, Q., Liu, K., Gao, G.F., 2022. Broader-species receptor binding and structural bases of Omicron SARS-CoV-2 to both mouse and palm-civet ACE2s. *Cell Discov* 8, 65.

- Li, W., Xu, Z., Niu, T., Xie, Y., Zhao, Z., Li, D., He, Q., Sun, W., Shi, K., Guo, W., Chang, Z., Liu, K., Fan, Z., Qi, J., Gao, G.F., 2024. Key mechanistic features of the trade-off between antibody escape and host cell binding in the SARS-CoV-2 Omicron variant spike proteins. *EMBO J.* 43, 1484–1498.
- Liu, K., Pan, X., Li, L., Yu, F., Zheng, A., Du, P., Han, P., Meng, Y., Zhang, Y., Wu, L., Chen, Q., Song, C., Jia, Y., Niu, S., Lu, D., Qiao, C., Chen, Z., Ma, D., Ma, X., Tan, S., Zhao, X., Qi, J., Gao, G.F., Wang, Q., 2021. Binding and molecular basis of the bat coronavirus RaTG13 virus to ACE2 in humans and other species. *Cell* 184, 3438–3451.e10.
- Liu, Y., Hu, G., Wang, Y., Ren, W., Zhao, X., Ji, F., Zhu, Y., Feng, F., Gong, M., Ju, X., Zhu, Y., Cai, X., Lan, J., Guo, J., Xie, M., Dong, L., Zhu, Z., Na, J., Wu, J., Lan, X., Xie, Y., Wang, X., Yuan, Z., Zhang, R., Ding, Q., 2021. Functional and genetic analysis of viral receptor ACE2 orthologs reveals a broad potential host range of SARS-CoV-2. *Proc. Natl. Acad. Sci. U. S. A.* 118, e2025373118.
- Niu, S., Wang, J., Bai, B., Wu, L., Zheng, A., Chen, Q., Du, P., Han, P., Zhang, Y., Jia, Y., Qiao, C., Qi, J., Tian, W.X., Wang, H.W., Wang, Q., Gao, G.F., 2022. Molecular basis of cross-species ACE2 interactions with SARS-CoV-2-like viruses of pangolin origin. *EMBO J.* 41, e109962.
- Peng, R., Wu, L.A., Wang, Q., Qi, J., Gao, G.F., 2021. Cell entry by SARS-CoV-2. *Trends Biochem. Sci.* 46, 848–860.
- Petersen, E.F., Goddard, T.D., Huang, C.C., Couch, G.S., Greenblatt, D.M., Meng, E.C., Ferrin, T.E., 2004. UCSF Chimera—a visualization system for exploratory research and analysis. *J. Comput. Chem.* 25, 1605–1612.
- Pickering, B., Lung, O., Maguire, F., Kruczkiewicz, P., Kotwa, J.D., Buchanan, T., Gagnier, M., Guthrie, J.L., Jardine, C.M., Marchand-Austin, A., Massé, A., McClinchey, H., Nirmalarajah, K., Aftanas, P., Blais-Savoie, J., Chee, H.Y., Chien, E., Yim, W., Banete, A., Griffin, B.D., Yip, L., Goolia, M., Suderman, M., Pinette, M., Smith, G., Sullivan, D., Rudar, J., Vernygora, O., Adey, E., Nebroski, M., Goyette, G., Finzi, A., Laroche, G., Ariana, A., Vahkal, B., Côté, M., McGeer, A.J., Nituch, L., Mubareka, S., Bowman, J., 2022. Divergent SARS-CoV-2 variant emerges in white-tailed deer with deer-to-human transmission. *Nat. Microbiol.* 7, 2011–2024.
- Porter, S.M., Hartwig, A.E., Bielefeldt-Ohmann, H., Bosco-Lauth, A.M., Root, J.J., 2022. Susceptibility of wild canids to SARS-CoV-2. *Emerg. Infect. Dis.* 28, 1852–1855.
- Punjani, A., Rubinstein, J.L., Fleet, D.J., Brubaker, M.A., 2017. cryoSPARC: algorithms for rapid unsupervised cryo-EM structure determination. *Nat. Methods* 14, 290–296.
- Rao, X., Zhao, R., Tong, Z., Guo, S., Peng, W., Liu, K., Li, S., Wu, L., Tong, J., Chai, Y., Han, P., Wang, F., Jia, P., Li, Z., Zhao, X., Li, D., Zhang, R., Zhang, X., Zou, W., Li, W., Wang, Q., Gao, G.F., Wu, Y., Dai, L., Gao, F., 2023. Defining a de novo non-RBM antibody as RBD-8 and its synergistic rescue of immune-evaded antibodies to neutralize Omicron SARS-CoV-2. *Proc. Natl. Acad. Sci. U. S. A.* 120, e2314193120.
- Tang, L., Zhang, D., Han, P., Kang, X., Zheng, A., Xu, Z., Zhao, X., Wang, V.Y., Qi, J., Wang, Q., Liu, K., Gao, G.F., 2022. Structural basis of SARS-CoV-2 and its variants binding to intermediate horseshoe bat ACE2. *Int. J. Biol. Sci.* 18, 4658–4668.
- Wang, M., Jing, H.Q., Xu, H.F., Jiang, X.G., Kan, B., Liu, Q.Y., Wan, K.L., Cui, B.Y., Zheng, H., Cui, Z.G., Yan, M.Y., Liang, W.L., Wang, H.X., Qi, X.B., Li, Z.J., Li, M.C., Chen, K., Zhang, E.M., Zhang, S.Y., Hai, R., Yu, D.Z., Xu, J.G., 2005. Surveillance on severe acute respiratory syndrome associated coronavirus in animals at a live animal market of Guangzhou in 2004. *Zhonghua Liuxingbingxue Zazhi* 26, 84–87 (In Chinese).
- Wang, Q., Zhang, Y., Wu, L., Niu, S., Song, C., Zhang, Z., Lu, G., Qiao, C., Hu, Y., Yuen, K.Y., Wang, Q., Zhou, H., Yan, J., Qi, J., 2020. Structural and functional basis of SARS-CoV-2 entry by using human ACE2. *Cell* 181, 894–904.e9.
- Wang, K., Pan, Y., Wang, D., Yuan, Y., Li, M., Chen, Y., Bi, L., Zhang, X.E., 2023. Altered hACE2 binding affinity and S1/S2 cleavage efficiency of SARS-CoV-2 spike protein mutants affect viral cell entry. *Virologica Sinica* 38, 595–605.
- World Organization for Animal Health (WOAH) (WOAH), 2023. SARS-CoV-2 in animals—situation-report-22/. <https://www.woah.org/en/document/sars-cov-2-in-animals-situation-report-22/>. (Accessed 30 June 2023).
- Wu, L., Chen, Q., Liu, K., Wang, J., Han, P., Zhang, Y., Hu, Y., Meng, Y., Pan, X., Qiao, C., Tian, S., Du, P., Song, H., Shi, W., Qi, J., Wang, H.W., Yan, J., Gao, G.F., Wang, Q., 2020. Broad host range of SARS-CoV-2 and the molecular basis for SARS-CoV-2 binding to cat ACE2. *Cell Discov* 6, 68.
- Xu, Z., Kang, X., Han, P., Du, P., Li, L., Zheng, A., Deng, C., Qi, J., Zhao, X., Wang, Q., Liu, K., Gao, G.F., 2022a. Binding and structural basis of equine ACE2 to RBDs from SARS-CoV, SARS-CoV-2 and related coronaviruses. *Nat. Commun.* 13, 3547.
- Xu, Z., Liu, K., Gao, G.F., 2022b. Omicron variant of SARS-CoV-2 imposes a new challenge for the global public health. *Biosaf. Health* 4, 147–149.
- Yan, R., Zhang, Y., Li, Y., Xia, L., Guo, Y., Zhou, Q., 2020. Structural basis for the recognition of SARS-CoV-2 by full-length human ACE2. *Science (New York, N.Y.)* 367, 1444–1448.
- Zhang, Z., Zhang, Y., Liu, K., Li, Y., Lu, Q., Wang, Q., Zhang, Y., Wang, L., Liao, H., Zheng, A., Ma, S., Fan, Z., Li, H., Huang, W., Bi, Y., Zhao, X., Wang, Q., Gao, G.F., Xiao, H., Tong, Z., Qi, J., Sun, Y., 2021. The molecular basis for SARS-CoV-2 binding to dog ACE2. *Nat. Commun.* 12, 4195.
- Zhao, X., Zheng, A., Li, D., Zhang, R., Sun, H., Wang, Q., Gao, G.F., Han, P., Dai, L., 2021. Neutralisation of ZF2001-elicited antisera to SARS-CoV-2 variants. *Lancet Microbe* 2, e494.
- Zhao, Z., Xie, Y., Bai, B., Luo, C., Zhou, J., Li, W., Meng, Y., Li, L., Li, D., Li, X., Li, X., Wang, X., Sun, J., Xu, Z., Sun, Y., Zhang, W., Fan, Z., Zhao, X., Wu, L., Ma, J., Li, O.Y., Shang, G., Chai, Y., Liu, K., Wang, P., Gao, G.F., Qi, J., 2023. Structural basis for receptor binding and broader interspecies receptor recognition of currently circulating Omicron sub-variants. *Nat. Commun.* 14, 4405.
- Zheng, S.Q., Palovcak, E., Armache, J.P., Verba, K.A., Cheng, Y., Agard, D.A., 2017. MotionCor2: anisotropic correction of beam-induced motion for improved cryo-electron microscopy. *Nat. Methods* 14, 331–332.
- Zhu, N., Zhang, D., Wang, W., Li, X., Yang, B., Song, J., Zhao, X., Huang, B., Shi, W., Lu, R., Niu, P., Zhan, F., Ma, X., Wang, D., Xu, W., Wu, G., Gao, G.F., Tan, W., China Novel Coronavirus Investigating and Research Team, 2020. A novel coronavirus from patients with pneumonia in China, 2019. *N. Engl. J. Med.* 382, 727–733.